Enhanced activation process of persulfate by mesoporous carbon for degradation of aqueous organic pollutants: Electron transfer mechanism

Lin Tang[a,b,*], Yani Liu[a,b], Jiajia Wang[a,b], Guangming Zeng[a,b,*], Yaocheng Deng[a,b], Haoran Dong[a,b], Haopeng Feng[a,b], Jingjing Wang[a,b], Bo Peng[a,b]

[a] College of Environmental Science and Engineering, Hunan University, Changsha, 410082, China
[b] Key Laboratory of Environmental Biology and Pollution Control, Hunan University, Ministry of Education, Changsha 410082, China

ARTICLE INFO

ABSTRACT

Metal-free catalysis for green degradation of aqueous organic pollutants has caused extensive concern in recent years. In this study, hexagonally-ordered mesoporous carbon (CMK-3) was applied to activate persulfate (PS) for the degradation of 2,4-dichlorophenol (2,4-DCP) with superior removal rate of 90% in 20 min. The high catalytic efficiency was probably ascribed to the accelerated electron transfer resulting from the large adsorption capacity of CMK-3. It was found that specific surface areas (SSA), defective sites and functional groups on the activator were highly related to its catalytic efficiency and passivation. Compared to other nanocarbons, CMK-3 had better reusability due to its ordered mesoporous structure with large SSA and high defective degrees. For the first time, a two-pathway mechanism was proposed for metal-free activation process of PS, indicating that radical and non-radical oxidation worked together in PS activation for complete 2,4-DCP decomposition, and non-radical pathway played a dominant role while radical pathway was critical in accelerating the reaction. $\cdot OH$, $SO_4 \cdot^-$ and $O_2 \cdot^-$ all took part in the radical oxidation process, in which the contribution of $\cdot OH$ was dominant. Besides, high decomposition efficiency was also achieved in pharmaceutical wastewater treatment by the CMK-3/PS system. This research proposed a new electron transfer mechanism for metal-free activation process of PS, which can provide a theoretical support for further studies.

1. Introduction

In recent decades, advanced oxidation processes (AOPs), such as Fenton reactions and sulfate radical-based AOPs (SR-AOPs), have been widely used in the removal of aqueous organic contaminants for their remarkable treatment efficiency. For traditional Fenton reaction, in a typical process, ferrous ions (Fe^{2+}) are used as homogeneous catalysts to stimulate H_2O_2 to generate hydroxyl radials ($\cdot OH$) for AOPs [1,2]. However, this process suffers from some limitations, such as strict requirement for acidic conditions (pH 2–4), production of large amount of sludge and the leaching of metal ions [3,4]. As promising alternatives, SR-AOPs could utilize peroxymonosulfate (PMS) or persulfate (PS) to generate free radicals (e.g. $SO_4 \cdot^-$ and $\cdot OH$) to oxidize organic contaminants to CO_2 and H_2O [5]. Compared with liquid H_2O_2, solid persulfate is more stable with lower price ($0.74/kg) vs PMS ($2.2/kg) or H_2O_2 ($1.5/kg), and is easier to transport and store [6]. Besides, sulfate radical ($SO_4 \cdot^-$) is a powerful one-electron oxidant with a high standard redox potential of $+2.60$ V vs normal hydrogen electrode (NHE) [7], comparable to that of $\cdot OH$ ($+2.80$ V vs NHE) [8], while its

lifetime is longer ($t_{1/2} = 30$–$40\,\mu s$ vs $t_{1/2} \leq 1\,\mu s$ of $\cdot OH$), allowing excellent electron transfer and contact with target pollutants [9]. In recent decades, SR–AOPs have been proved to be an effective approach for removing various recalcitrant pollutants in water (e.g. volatile organic compounds, endocrine disruptors, cyanotoxins as well as pharmaceuticals and their metabolites) [5], and therefore draw great attention.

In general, peroxymonosulfate or persulfate without activation presents low oxidative potential for organic decomposition (except the Elbs and Boyland-Sims reactions) [10]. In order to avoid too much energy or chemical inputs in homogeneous activation system (e.g. UV irradiation [11,12], heating [13,14], ultrasound [15], base [16], phenols [17], quinones [18], metal ions [19,20]), effective heterogeneous systems based on metal/metal oxides catalysts (e.g. Fe- [7], Co- [21], Mn- [22], and Cu-based [23] catalysts) are broadly investigated, in which catalysts can be easily separated from the treated water for recycling. However, the problem of metal leaching still exists. As a result, environmental friendly metal-free catalysts would be highly in demand in terms of sustainable development.

In the last few years, some emerging nanocarbons have been

---

reported to effectively activate PMS or PS for oxidation of organics, along with their great superiorities in large surface area, high conductivity and good stability. Wang and Sun's group utilized activated carbon supported cobalt catalysts to activate PMS for the oxidation of phenol and found that activated carbon showed a remarkable activity in PMS activation [24]. And then, they firstly discovered that chemically reduced graphene oxide (rGO), a metal-free catalyst, can effectively activate PMS [25]. After that, various nanocarbons, such as carbon nanotubes, fullerene and nanodiamonds were also investigated for SR-AOPs in water [26–31]. Compared with other nanocarbons, ordered mesoporous carbon possesses larger surface area and unique mesoporous structure, resulting in excellent physicochemical properties, which makes it become a promising catalyst candidate in SR-AOPs. Up to now, although ordered mesoporous carbon was applied for comparisons with other nanocarbons in SR-AOPs in a few reports [29,31], exhibiting superior catalytic performances, its activation mechanism was still not clear enough.

Usually, SR-AOPs involve the generation of free radicals to attack the pollutants. However, non-radical oxidation pathways have also been reported in SR-AOPs recently, in which the organics can be degraded without radicals. Some researches proposed that instead of radicals, singlet oxygen ($^1O_2$) could be produced during the activation process of PMS or PS for the decomposition of organics in some systems [32,33]. Other studies reported that PS (or PMS) was likely to bind onto the surface of catalyst to form reactive complexes, followed by a rapid reaction with organics, in which no radicals were involved [6,34]. Thus, the mechanism in SR-AOPs still remains blurred and largely unexplored.

Herein, in order to reveal the mechanism involved in mesoporous carbon based SR-AOPs, for the first time, we used CMK-3 (hexagonally-ordered mesoporous carbon) to activate PS for the catalytic oxidation of organic pollutants. The degradation of 2,4-dichlorophenol (2,4-DCP), a frequently detected organic contaminant in water, in CMK-3/PS system under various experimental conditions was investigated. Considering the high adsorption capacity of CMK-3, the relationship between adsorption and oxidation process was discussed. The active sites and reasons for passivation of CMK-3 were revealed by analyzing the changes of CMK-3 before and after reaction. Furthermore, a two-pathway mechanism was proposed for the first time, based on the results from radical quenching test, electron spin resonance (ESR) spectroscopy, PS decomposition and linear sweep voltammetry (LSV). Real pharmaceutical wastewater samples were also employed to evaluate the application prospect of CMK-3/PS system.

2. Materials and methods

2.1. Materials and chemicals

The mesoporous silicon templates (SBA-15) were firstly prepared according to a conventional hydrothermal synthesis method as reported [35]. Mesoporous carbon (CMK-3) was self-synthesized via an impregnation method with slight alternations [36]. The synthesis procedures of CMK-3 and details about other chemicals were provided in Supporting Information (SI).

2.2. Characterization

The morphological information and structure of CMK-3 were obtained by scanning electronic microscopy (SEM, Hitachi S-4800) and high-resolution transmission electron microscopy (HRTEM, JEM-3010). The specific surface area (SSA) and pore size distribution were acquired from nitrogen sorption isotherms on a Quantachrome Autosorb AS-1. Raman spectra were performed on an argon ion laser equipped ISA dispersive Raman spectroscopy at 514 nm. Surface functional groups of CMK-3 were analyzed by a Fourier-transform infrared spectroscopy (FTIR) on a PerkinElmer instrument (Spectrum GX, USA) within the

2000–400 cm^{-1} region at a 4 cm^{-1} resolution (KBr pellets). X-ray photoelectron spectroscopy (XPS) was used to probe the surface chemistry and chemical states of elements by a Thermo Escalab 250 instrument under an Al-Kα X-ray radiation. All binding energies were calibrated with C1s at 284.5 eV and fitted with CasaXPS software.

2.3. Catalytic activity tests

The catalytic oxidation of 2,4-DCP by CMK-3 activated PS was carried out in a thermostatic shaker. All batch experiments were performed in conical flasks with a shaking rate at 200 rpm, keeping the temperature at 298 K. Typically, considering the superior adsorption performance of CMK-3, CMK-3 was first dispersed into 2,4-DCP solution (200 mg/L, pH 6.37 without any buffering) and shaken for 1 h to achieve adsorption-desorption equilibrium. Then a certain amount of PS was added to initiate the degradation process. In general, unless otherwise noted, the amounts of CMK-3 and PS are 0.2 g/L and 2 g/L, respectively. 0.1 M HNO$_3$ or NaOH was used to adjust the pH of solution. At each time interval, the reaction solution was withdrawn, filtered and then injected into a vial containing 0.5 mL of methanol to scavenge the reactive species and quench the further oxidation reaction. The experiment on real water sample was conducted the same as above. For the stability tests, CMK-3 was collected after each run and washed with ethanol and water for three times and dried at 333 K for reuse. To investigate the roles of reactive radicals, certain amounts of radical scavengers (methanol (MeOH) and tert-butyl-alcohol (TBA), calibrated by molar ratio MeOH/PS or TBA/PS) were added into the reactions to scavenge SO$_4$·$^-$ and ·OH. 1,4-benzoquinone (BQ) and sodium azide (NaN$_3$) were used as the quencher for O$_2$·$^-$ and $^1O_2$, respectively. Most experimental samples were performed in duplicate or triplicate, and the average values were used with standard deviations represented by error bars in corresponding graphs.

2.4. Analytical methods

The concentration of 2,4-DCP was analyzed by a high performance liquid chromatography (HPLC, Agilent 1200) with a C18 column (5.0 μm, 4.6 mm × 250 mm) and a UV detector set at 285 nm. The mobile phase was methanol/water (60:40, v/v) with a flow rate of 1.0 mL/min. PS concentration were measured using the modified spectrophotometric method based on iodometric titration method, which was proposed by Liang et al. [37]. The generated active radicals were examined on a Bruker ER200-SRC spectrometer with 5,5-di-methyl-1-pyrroline N-oxide (DMPO) as spin-trapping agent. The detection of SO$_4$·$^-$ and ·OH were conducted in ultrapure water while the detection of O$_2$·$^-$ was conducted in solution containing ethanol. The concentration of total organic carbon (TOC) was measured using a Shimadzu TOC-VCPH analyzer. The real water samples were characterized by three-dimensional excitation-emission matrix (3D-EEM) fluorescence spectroscopy on F-4600 FL spectrophotometer (Hitachi, Japan). Linear Sweep Voltammetry (LSV) measurement and electrochemical impedance spectroscopy (EIS) was carried out in a CHI 660C electrochemical analyzer (CHI-660C, China). The by-products of 2,4-DCP after CMK-3/PS treatment were identified by GC/MS. The details for 3D-EEM, LSV measurement and GC–MS method were provided in SI.

2.5. Real water sample treatment

The pharmaceutical wastewater sample generated from the bufex-amac (a nonsteroidal anti-inflammatory and analgesic drug) production process was collected from Liuyang Bio-medicine Garden, in Hunan Province, China. The main contents in the wastewater include bufex-amac, methanol, ethanol, hydroxylamine, 1-bromobutane and other organic matters. The sample was filtered by a 0.45 μm PES membrane prior to use. Other properties of the wastewater sample are presented in Table S1.
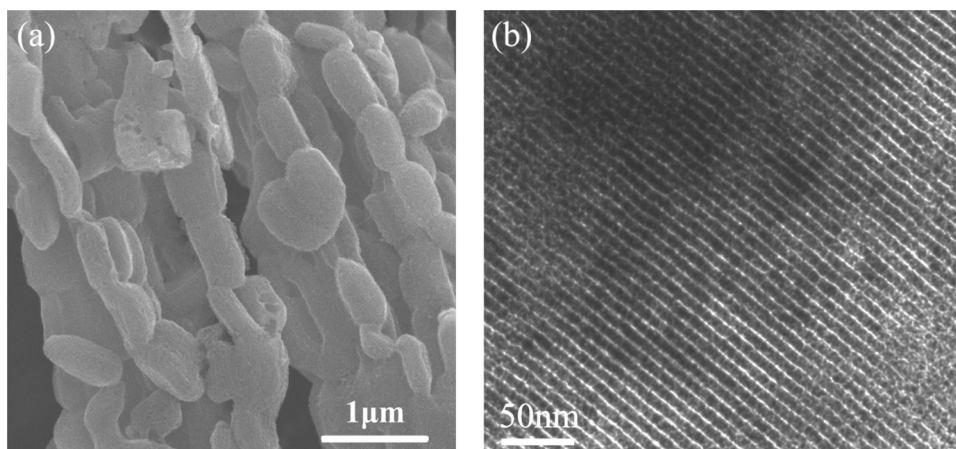
Fig. 1. (a) SEM image and (b) HRTEM image of CMK-3.

3. Results and discussion

3.1. Catalytic performances of CMK-3

Before catalysis tests, the morphological information and structure of self-synthesized CMK-3 were revealed by SEM (Fig. 1a) and HRTEM (Fig. 1b). It was clearly observed that the carbon materials consisted of many rod-type structures, which were aggregated into wheat-like macrostructures, and the average length of each rod was about 0.8 μm. The well-ordered stripe-like structures of mesopores were clearly shown in HRTEM image. These characteristics accorded well with the CMK-3 synthesized in our previous work [38–40]. Owing to the uniform mesoporous structure, large adsorption capacity and more exposed active sites can be expected, which is beneficial for CMK-3 to activate PS.

The catalytic performance of CMK-3/PS system on 2,4-DCP degradation and the corresponding kinetic behaviors were investigated with various reaction parameters (e.g. the dosage of persulfate and catalyst, solution pH and temperature). Firstly, the influence of the dosage of PS and CMK-3 was studied, and results were presented in Fig. 2a and b. An adsorption study of 2,4-DCP on CMK-3 (0.2 g/L) was carried out for 3 h without PS addition. The adsorption process could achieve equilibrium in 1 h with about 50% of 2,4-DCP (200 mg/L) removed. The superior adsorption performance may be attributed to the porous structure and large specific surface area (SSA) of CMK-3. Moreover, the edge defects with versatile oxygen groups on the surface of CMK-3 also played crucial roles to enhance the chemisorption for binding 2,4-DCP [41]. More information about the adsorption process was provided in SI (adsorption kinetic analysis, Fig S1, Table S2). In order to dispel the effect of adsorption, PS was added after the adsorption reaching equilibrium in 1 h in the following experiments. It could be clearly observed in Fig. 2a that after adding PS (2 g/L), the concentration of 2,4-DCP had a distinct decrease with removal rate of 90% in 20 min, and it could be completely removed after 2 h reaction. It means that besides adsorption, a chemical reaction actually occurred at high rate, and it could be affected by the dosage of PS. Pseudo-first-order kinetics based on Langmuir–Hinshelwood model (Eq. (1)) was used to fit the 2,4-DCP degradation curves, resulting in high value of regression coefficients (R^2) (Fig. S2). The pseudo-first-order rate constant, k_{obs}, was obtained by linear regression of Eq. (2), which was derived from Eq. (1) when $t = 0$, $C = C_0$:

$$-dC/dt = k_{obs}C \tag{1}$$

$$\ln(C_t/C_0) = -k_{obs}t \tag{2}$$

where C_0 and C_t are the initial 2,4-DCP concentration and the concentration at time t, respectively.

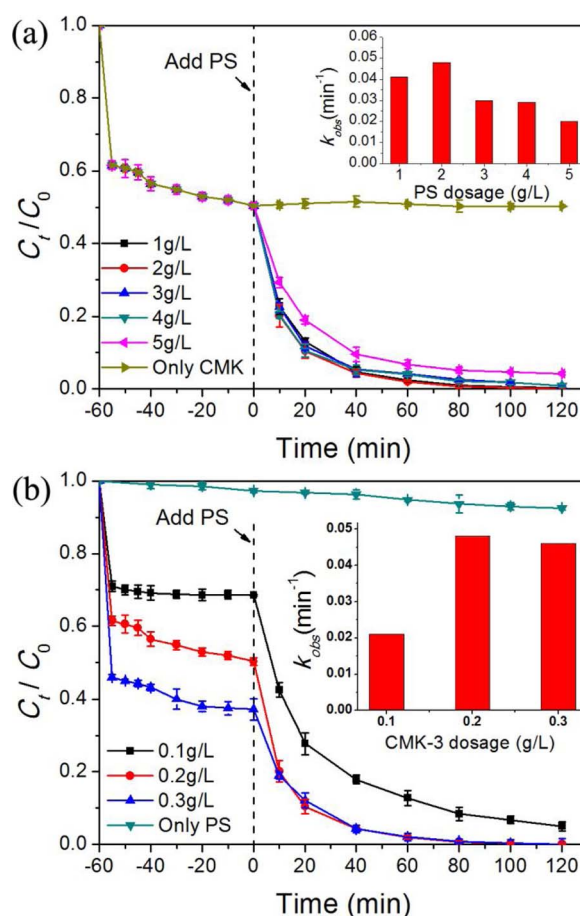When PS dosage increased from 1 g/L to 2 g/L, the k_{obs} increased

Fig. 2. The effects of (a) PS dosage ([CMK-3] = 0.2 g/L) and (b) catalyst dosage ([PS] = 2 g/L) on 2,4-DCP degradation. Experimental conditions: [2,4-DCP] = 200 mg/L, [Temp] = 298 K. Insets are the corresponding changes of pseudo-first-order rate constant.

from 0.041 min^{-1} to 0.048 min^{-1} (Fig. S2a). This was mainly because a larger dosage of PS could provide more reactive radicals for reaction [29]. However, when the amount of PS continued to increase, k_{obs} decreased rather than increased, which might be ascribed to the self-quenching effect among excessive radicals [42]. Additionally, PS alone can hardly oxidize 2,4-DCP without activation as removal rate was only 7% after 3 h (Fig. 2b). Herein, CMK-3 acted as an activator, and an enhanced 2,4-DCP degradation efficiency was achieved with the increase of CMK-3 dosage (Figs. 2b and S2b) due to more active sites provided. It was also noteworthy that when CMK-3 dosage reached to

0.3 g/L, k_{obs} did not increase anymore, which may be limited by the dosage of PS.

The effects of temperature were further investigated as shown in Fig. S3. At 298 K, 2,4-DCP could be removed in 2 h. When temperature increased to 318 K, 2,4-DCP could be completely removed in 40 min. It could be concluded that PS activation processes were improved with elevated temperatures as k_{obs} increased remarkably with increasing temperature (Fig. S3a and b). Two reasons could account for this phenomenon. On one hand, higher temperature could accelerate the decomposition of PS and therefore facilitate the degradation of 2,4-DCP, as increasing temperature enhanced the removal rate of 2,4-DCP by PS alone (Fig. S3c). On the other hand, adsorption process was also promoted with elevated temperature (Fig. S3a), which favored electron transfer between CMK-3 and PS. The activation energy of 2,4-DCP degradation on CMK-3/PS was evaluated to be 49.3 kJ/mol using the Arrhenius equation (inset in Fig. S3a).

3.2. Stability tests

The stability of catalytic materials for continuous PS activation is very important in application. Four-cycle experiments were conducted to demonstrate the reusability of CMK-3/PS system for the removal of 2,4-DCP with results shown in Figs. 3a and S4. Fresh CMK-3 could completely remove 2,4-DCP in 2 h reaction, and it demonstrated good reusability providing 98.8% 2,4-DCP removal efficiency in the 2nd run, although the k_{obs} decreased. Moreover, 87% and 72% of 2,4-DCP were removed in the 3rd and 4th runs, respectively. In previous studies, metal catalysts usually showed poor reusability for PS activation, owing to the irreversibility of homogeneous metal ions. In general, the deactivation of metal oxides was mainly ascribed to the coverage of intermediates and changes of surface crystal structure. For zero-valent iron

(ZVI), ferric hydroxide or ferrous sulfate were easily covered on the surface, and thus prevented the further activation of PS [43]. However, passivation of nanocarbons for PS activation was slightly different, which was usually related to the altered surface chemistry and structure of carbocatalysts [26,42].

In order to identify the changes of SSA and pore structure of CMK-3 before and after catalytic oxidation reactions, nitrogen adsorption-desorption isotherms were recorded, as shown in Fig. 3b. The two isotherm curves (inset in Fig. 3b) both exhibited type IV feature, revealing the typical mesoporous features of CMK-3. The pore size distributions curves further confirmed that the pore sizes of CMK-3 are mainly distributed around 4–5 nm, indicating the uniform mesoporous structure, corresponding to the HRTEM image. Meanwhile, it could be clearly observed that the pore size decreased after the second run. The changes of specific pore structure parameters were listed in Table S3. Owing to abundant mesopores, CMK-3 possessed high SSA of 900.39 m^2/g and large pore volume of 1.32 cm^3/g. These properties not only facilitate the adsorption of pollutants and enhance mass transfer process, but also help to expose more active sites for surface catalytic reactions [26], which creates good conditions for CMK-3 to activate PS. However, due to the adsorption of intermediates, there were distinct decreases in SSA (decreased to 505.54 m^2/g) after the second catalytic test, along with decreases of pore size and pore volume, which affected the subsequent adsorption ability. It was further confirmed in Fig. 3a with a decrease of adsorption. As a result, the active sites were covered, and electron transfer process was blocked, leading to the deactivation of CMK-3.

One important parameter to evaluate the crystalline structure of carbon materials is the I_D/I_G (representing the disorder degree), which could be obtained in Raman spectra. Thus, the Raman curves of CMK-3 before and after cycling test were presented in Fig. 3c. Two
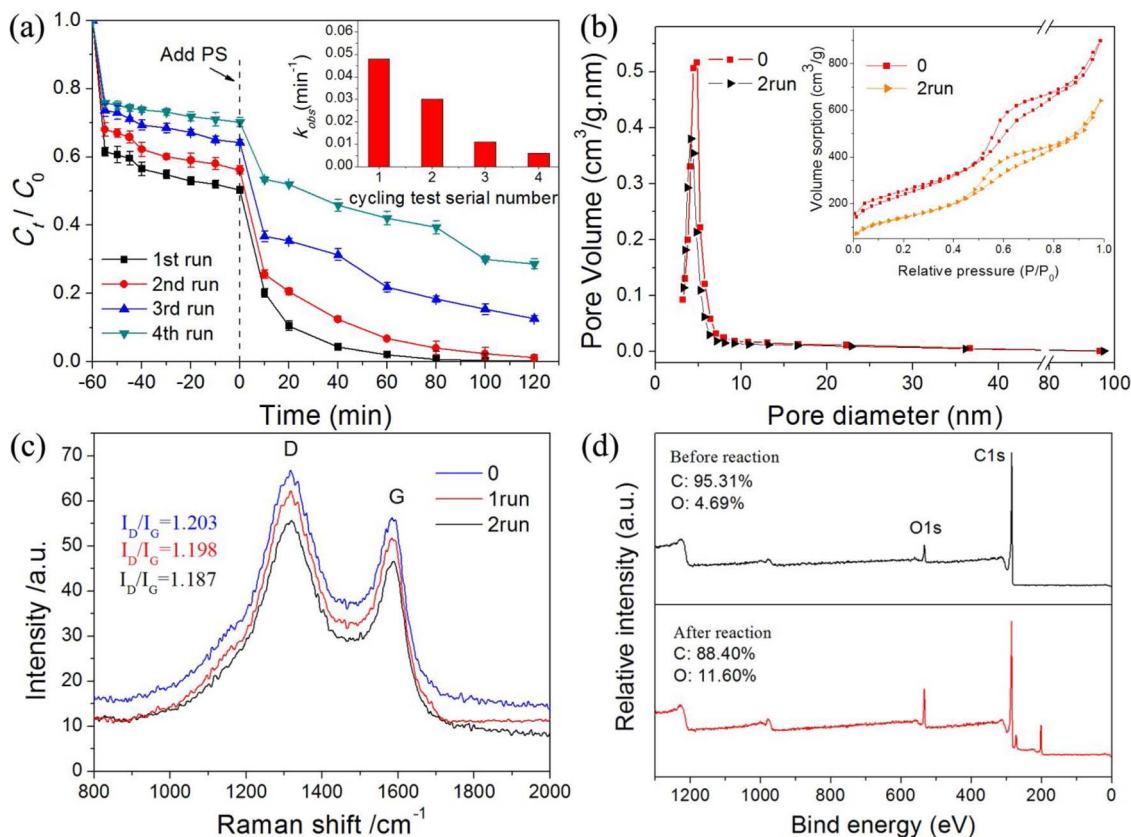

Fig. 3. (a) Stability tests of CMK-3 and inset is the corresponding pseudo-first-order rate constant, [2,4-DCP] = 200 mg/L, [PS] = 2 g/L; [CMK-3] = 0.2 g/L; [Temp] = 298 K; (b) Pore distribution curves of pristine CMK-3 and CMK-3 after the second recyclability test, and inset is the corresponding nitrogen adsorption–desorption isotherms; (c) Raman spectra of pristine CMK-3 and CMK-3 after the first and second recyclability tests; (d) XPS survey of CMK-3 before and after reaction.
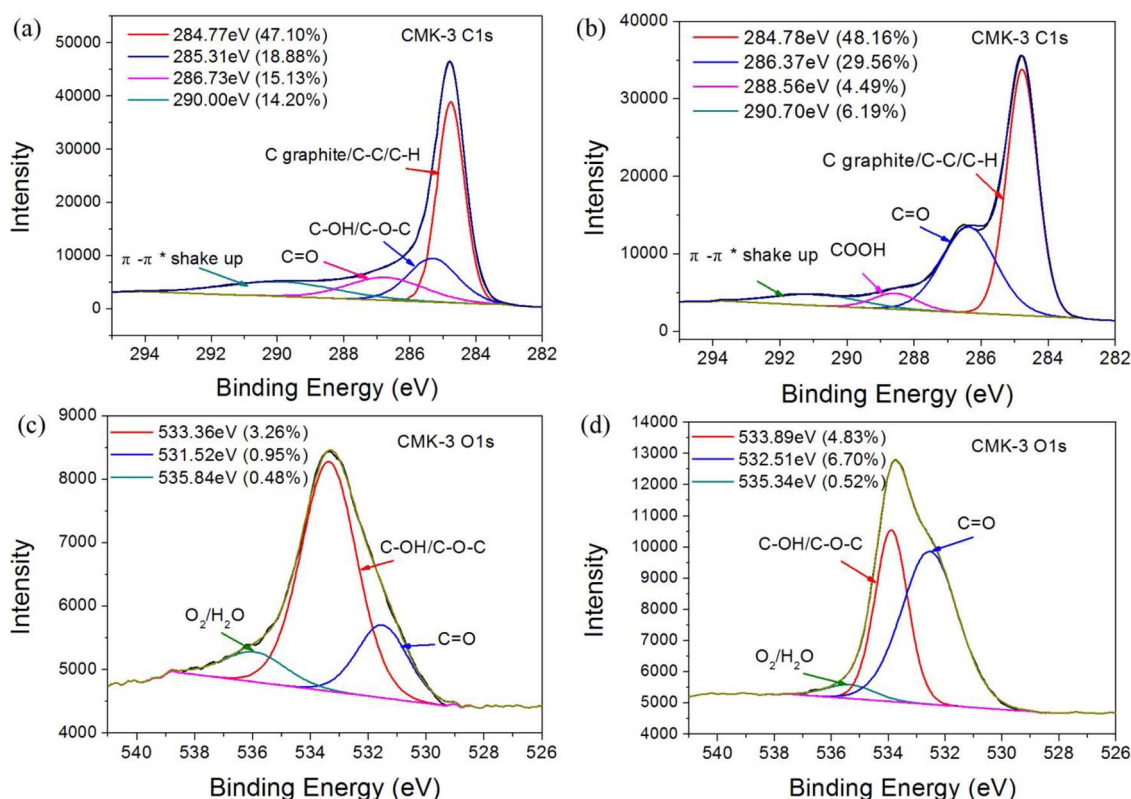
Fig. 4. (a) C1s and (c) O1s high resolution scans of CMK-3 before reaction; (b) C1s and (d) O1s high resolution scans of CMK-3 after reaction.

characteristic peaks of carbon nanomaterial could be clearly observed. The D peak near 1310 cm^{-1} reflected the degree of disorder, while the G peak at 1580 cm^{-1} reflected the level of graphitization [44]. Interestingly, the I_D/I_G ratio progressively decreased along with the increasing of cycling times. After the second run, the I_D/I_G ratio changed to 1.187 compared to the original 1.203, suggesting the decrease of defective degrees, which may be attributed to the destruction of defective edges, changes of surface functional groups and the strong interaction between the adsorbed substances and sp^2 hybridized carbon system. Recently, Wang and Sun et al. found that the defective edges of nanocarbons could be active sites for phenol oxidation [26]. Here, we actually discovered the changes in defective degree after catalytic reaction and the trend corresponded well to the catalytic efficiency changes of CMK-3 in the first three cycling tests (Fig. 3a). This implied that the decrease of defective sites was one of the reasons for CMK-3 passivation, and defective sites did play important roles in catalytic reaction.

In addition, both XPS and FTIR spectra (Figs. 3d and S5) showed the altered surface chemistry (further discussed below) before and after stability tests, which also resulted in the passivation of CMK-3. Compared with other nanocarbons, such as carbon nanotubes (CNTS), cubic ordered mesoporous carbon (CMK-8), activated carbon (AC), reduced graphene oxide (rGO) and nitrogen doped reduced graphene oxide (N-rGO), the stability of CMK-3 is much better and similar to that of nanodiamond (AND), as shown in Table S4. This might be ascribed to the ordered mesoporous structure with large SSA and high defective degrees. One should be noted that compared with commercial metal-based systems such as electrochemical catalysis, the current stability of SR-AOPs activated by nanocarbons is still not good enough [42]. Thus, more research should be conducted to develop efficient and stable metal-free catalysis or to improve the property of carbon catalysts to replace metal catalysis for future applications.

3.3. The surface investigation of CMK-3

The edges of nanocarbons are terminated with hydrogen and oxygen atoms. Multitudinous oxygen groups, such as hydroxyl (C−OH), carbonyl (C=O), and carboxyl (−COOH), have been confirmed to exist on the surface of nanocarbons, which could affect the catalytic activity of carbon catalysts [26,29]. Owing to the nucleophilicity, electron rich-containing groups such as ketonic and quinone groups (C=O) could work as Lewis basic sites, playing important roles in selective catalytic reaction [31]. Duan et al. proposed that the asymmetric O−O bond in PMS molecules (HO−SO$_4^-$) could be weakened by the sp^2-hybridized carbon network with conjugated π systems. Then oxygen groups, especially the carbonyl (C=O) and edge defects, presenting a high redox potential, facilitated electron transfer from the catalyst to PMS to generate free radicals, and thus activated PMS for oxidation reactions [26,45]. Analogously, the essence of PS activation is the breaking-up of O−O (SO$_4$−SO$_4$) bond. Do the functional groups play similar roles in this process? In order to solve this problem, XPS and FTIR were utilized to probe the surface compositional information and functional groups.

Fig. 3d showed the XPS survey of CMK-3. Here, we can easily see that there were two distinct peaks centered at 284.8 eV and 533.2 eV with percentages of 95.31% and 4.69%, which were assigned to C1s and O1s, respectively. For comparison, the curve of CMK-3 after catalytic reactions was also presented. There were two new peaks appearing at 200 eV and 270 eV, which belonged to Cl2p and Cl2s, resulting from the adsorption of 2,4-DCP and its intermediates. It was interesting to find that the oxygen content increased from 4.69% to 11.6%, in accordance with other nanocarbons in previous studies [26,42], indicating the surface oxidation of CMK-3 during PS activation process. We proposed two possible reasons to explain this phenomenon: 1) as a bridge of electron transfer, surface functional groups were oxidized by donating electrons to activate PS; 2) the surface of CMK-3 was surrounded by a highly oxidative environment with large amount of radicals during catalytic reaction, resulting in surface oxidation. The increase of oxygen content would change the surface features of CMK-3

and thus affect the adsorption and catalytic behavior, as discussed in stability tests. The C1s high resolution scans were obtained to exhibit the details of functional groups as shown in Fig. 4a and b. A broad C1s peak of original CMK-3 could be fitted into four species with binding energies at 284.77, 285.31, 286.73 and 290 eV, which were assigned to C graphite/C−C/C−H, C−OH/C−O−C, C=O and π-π* shake up, respectively [29]. The C1s peak of CMK-3 after reaction was also divided into four sections at 284.78, 286.37, 288.56 and 290.7 eV, indicating C graphite/C−C/C−H, C=O, COOH and π-π* shake up, respectively. The corresponding O1s high resolution scans were also displayed in Fig. 4c and d. It should be noted that both C1s and O1s scans showed the decrease of C−OH/C−O−C and the increase of C=O after reaction, indicating the transformation between the two groups. Therefore, combining this phenomenon with the stability tests results, we proposed that instead of C=O, C−OH were more likely to act as active sites in CMK-3/PS system, as they were also electron-donating groups.

Fig S5 displayed the FTIR spectroscopy of various CMK-3 after adsorption and different reaction time with a wavenumber range of 2000–400 cm^{-1}. The broad peaks at 1573 cm^{-1} and 1260 cm^{-1} of original CMK-3 could be assigned to the C=C bonding of graphite C and C−O group [29]. As the oxygen content was very small (Fig. 3d), peaks of other oxygen groups were not observed. After the adsorption of 2,4-DCP without PS for 1 h, two new peaks appeared at 810 cm^{-1} and 1480 cm^{-1}, corresponding to out-of-plane bending vibration of C−H in phenyl ring and the stretching vibration of bonds in 2,4-DCP, respectively, indicating that 2,4-DCP was indeed attached to the surface of CMK-3. The adsorption of PS without pollutants was also conducted for comparison, and no peak at 810 cm^{-1} or 1480 cm^{-1} was observed. After the start of reaction, the two peaks decreased with the increase of reaction time, and many other peaks appeared, suggesting the decomposition of 2,4-DCP and generation of intermediates. These results implied that the degradation of 2,4-DCP not only happened in solution, but also occurred on the surface of CMK-3. In addition, the peak of S=O bond stretching also appeared at 1054 cm^{-1} after reaction [46], indicating that PS was decomposed to SO_4^{2-}, and a part of them were adsorbed to the surface of CMK-3.

3.4. Identification of radicals

In general, PS can be activated to generate free radicals to oxidize organic contaminants, namely, a radical process. However, non-radical oxidation processes have also been observed when CuO [6] and carbon nanotubes [34] were applied as activators in recent studies. Therefore, it is necessary to determine the generation of radicals in CMK-3/PS system.

Herein, radical quenching reaction was utilized to investigate the effects of radicals. $SO_4^{\cdot-}$ and ·OH are often considered as reactive species for pollutant oxidation in PS activation. Owing to the different reaction rate with radicals, *tert*-butyl-alcohol (TBA) and methanol (MeOH) are usually applied to distinguish the contribution of the two radicals. MeOH could be an effective quencher for both $SO_4^{\cdot-}$ and ·OH ($k_{SO4\cdot-} = 1.1 \times 10^7 M^{-1} s^{-1}$, $k_{\cdot OH} = 9.7 \times 10^8 M^{-1} s^{-1}$), while TBA is only effective for ·OH ($k_{\cdot OH} = 6 \times 10^8 M^{-1} s^{-1}$), not for $SO_4^{\cdot-}$ ($k_{SO4\cdot-} = 4 \times 10^5 M^{-1} s^{-1}$) [45,47]. According to the inhibition effects on reaction, roles of the two radicals in 2,4-DCP degradation will be clear. Results displayed in Fig. 5a, b and d showed that the existence of either MeOH or TBA inhibited the degradation of 2,4-DCP, with a dramatic decrease of k_{obs} from 0.048 min^{-1} to 0.017 min^{-1} (n[MeOH/PS] = 1000) and 0.018 min^{-1} (n[TBA/PS] = 1000), respectively. In addition, compared with that of TBA, the increase of MeOH concentration resulted in a relatively faster decrease of k_{obs}, indicating a stronger inhibiting ability of MeOH to the reaction. These results suggest that both $SO_4^{\cdot-}$ and ·OH were generated and took part in the reaction, while ·OH was relatively more dominant than $SO_4^{\cdot-}$ in the degradation of contaminant. Furthermore, 1,4-benzoquinone (BQ) was also added to determine the existence of superoxide anion radical

($O_2^{\cdot-}$), as the reaction rate constant was very rapid ($1.0 \times 10^9 M^{-1} s^{-1}$) [48]. Results in Fig. 5c showed that BQ could also slightly inhibit the reaction, as the calculated k_{obs} decreased to 0.021 min^{-1}. This indicates that $O_2^{\cdot-}$ also participated in 2,4-DCP decomposition but the contribution was inferior to that of ·OH.

The existence of radicals was further confirmed by electron spin resonance (ESR) spectroscopy, with DMPO as spin-trapping agent to capture the free radicals. As shown in Fig. 5e, the characteristic signals of DMPO-OH (hyperfine splitting constants of aN = aH = 14.9 G) and DMPO-SO₄ (aN = 13.2 G, aH = 9.6 G, aH = 1.48 G and aH = 0.78 G) were clearly seen [49]. The intensity of DMPO-OH was much higher than that of DMPO-SO₄, indicating a higher concentration of ·OH, which could support the result of quenching experiment that ·OH was relatively more dominant. In addition, six characteristic peaks of DMPO-OOH (the combination of $O_2^{\cdot-}$ and DMPO) could also be found in Fig. 5f, which further confirmed the existence of $O_2^{\cdot-}$ [50,51].

It is interesting to find that when the concentration of scavenger was relatively low (n[scavenger/PS] ≤ 200), the decrease of k_{obs} was fast; but when the ratio further increased, the decrease of k_{obs} was slower (Fig. 5d). A plausible explanation is that most radicals could be scavenged at a ratio as high as 200, so the further increase of scavenger did not make much difference. The slow reduction of k_{obs} in a ratio over 200 may be partly attributed to the coverage of MeOH or TBA on CMK-3 surface at high concentration, which hindered the access of persulfate and 2,4-DCP to CMK-3. It should be noted that although radical scavengers were excessive, only the reaction rate decreased significantly, while the removal efficiency did not change much (Fig. 5a–d). This implied that there also existed non-radical oxidation process in which the decomposition of 2,4-DCP could still proceed even when radicals were captured. Based on the results in Fig. 5, non-radical pathway may be more predominant in 2,4-DCP degradation, while radical pathway played an important role in accelerating the reaction. In addition, the degradation of 2,4-DCP was only slightly reduced in the presence of NaN₃ (Fig. 5c), a unique scavenger for $^1O_2$, suggesting the negligible contribution of $^1O_2$ in organic degradation.

The decomposition of PS under different conditions was revealed in Fig S6a. Obviously, PS decomposition is negligible (less than 3% in 120 min) in the solution of 2,4-DCP, while 8% of PS can be consumed when reacted with CMK-3 without 2,4-DCP, suggesting that PS could be activated by CMK-3. In addition, the consumption of PS could further increase to 11% when CMK-3 and 2,4-DCP both existed, which indicated the significant interaction among PS, 2,4-DCP and CMK-3, and the key roles of both pollutant and catalyst. Since only a small portion of PS was utilized in the reaction, the resulted solution was reused for 2,4-DCP degradation (Fig. S6b), and a fast degradation could also be achieved when the used CMK-3 was replaced with fresh one. When CMK-3 was not replaced, the removal rate of 2,4-DCP was decreased, which may be attributed to the deactivation of CMK-3, as the decomposition of PS also reduced (Fig. S6c). These results indicated that the consumption of PS in CMK-3/PS system was small, which was different from the rapid consumption in a nFe°/PS system [52], highlighting the difference in the activation mechanism.

3.5. Electron transfer pathways and influencing factors

On the basis of the above analysis, the mechanisms of catalytic oxidation of 2,4-DCP by CMK-3 activated PS are proposed as follows and shown in Scheme 1. Since $S_2O_8^{2-}$ itself was unable to produce ·OH, ·OH should be originated from H_2O or OH^-. However, persulfate cannot directly oxidize H_2O to generate ·OH without any assistance [53], and the direct oxidation of 2,4-DCP by PS was also very slow (Fig. 2b). It is reasonable to propose that the sp2-hybridized carbon network with defective edge sites and free-flowing π electrons on the surface of CMK-3, owing to unique electronic circumstance, were able to affect the electron configuration of PS and weaken the O−O bond to form metastable complexes (the active state of PS). There are two
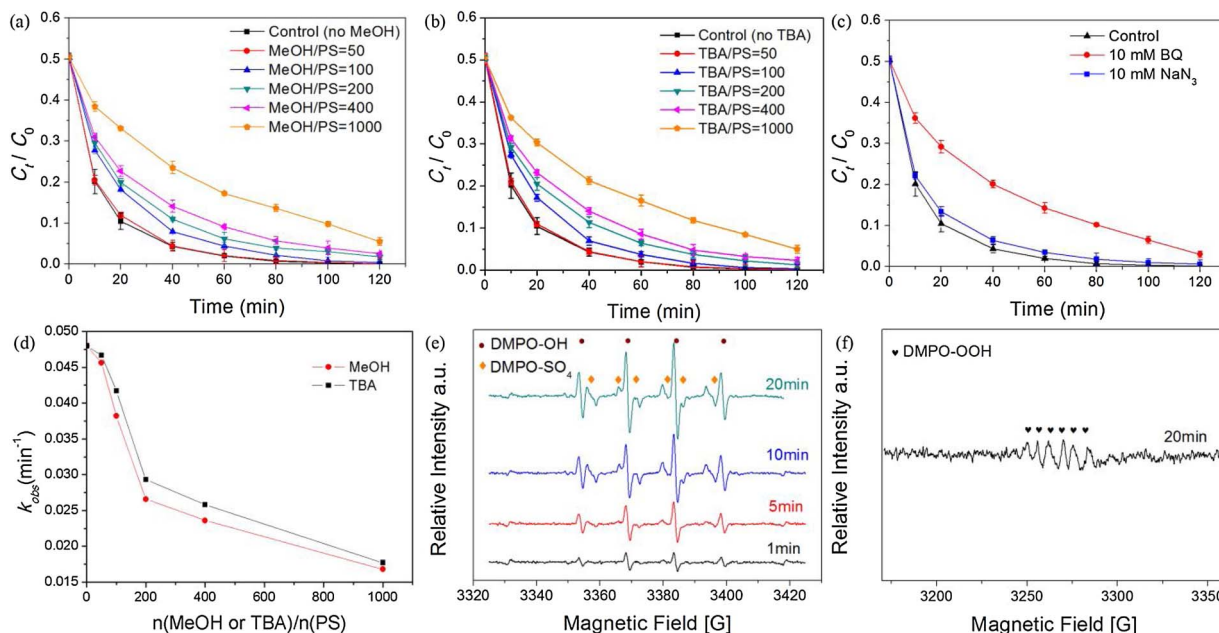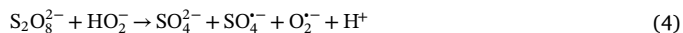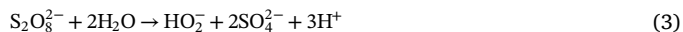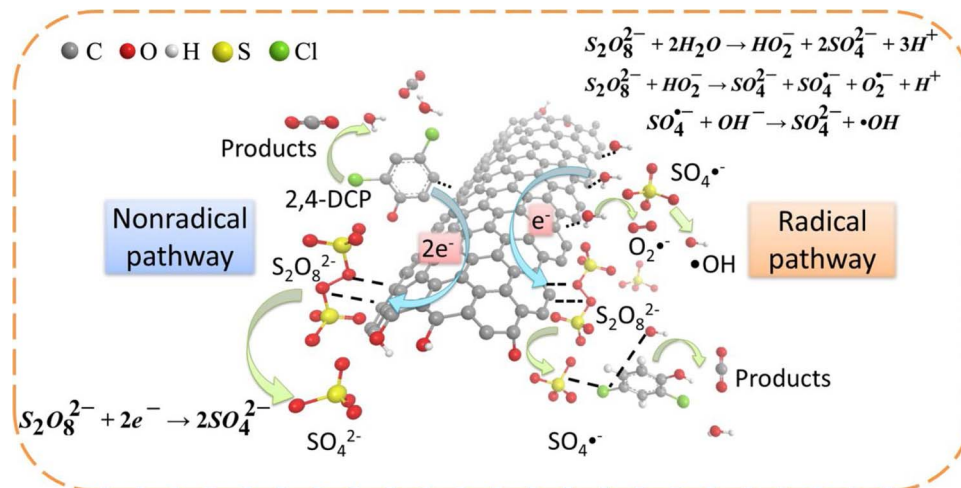
Fig. 5. Effects of (a) MeOH and (b) TBA on 2,4-DCP degradation at different molar ratio with PS, [2,4-DCP] = 200 mg/L, [PS] = 2 g/L, [CMK-3] = 0.2 g/L, [Temp] = 298 K. (c) Effects of PB (10 mM) and NaN$_3$ (10 mM) on 2,4-DCP degradation; (d) Effects of MeOH and TBA on the pseudo-first-order rate constants at different molar ratio with PS; (e–f) ESR spectra of PS activation by CMK-3.

possible pathways in the following evolution. On the one hand, the metastable complexes facilitated the hydrolysis of PS (Eq. (3)) [16,33], and then the HO$_2^-$ was quickly oxidized by another S$_2$O$_8^{2-}$ via one-electron transfer process (Eq. (4)), resulting in the generation of SO$_4$·$^-$ and O$_2$·$^-$. Here, carbon network played an important role as the electron transfer mediator. SO$_4$·$^-$ could also be partly converted to ·OH via Eq. (5) with high rate of 7.0×10^7 M^{-1} s^{-1} [54]. The generated SO$_4$·$^-$, O$_2$·$^-$ and ·OH would then take part in the oxidation of 2,4-DCP. On the other hand, as more significant decomposition of PS occurred when 2,4-DCP coexisted in the solution than that in the absence of 2,4-DCP (Fig. S6a), pollutant may also directly act as electron donor for metastable complexes. When 2,4-DCP with abundant electron approached to the activated PS molecule, a ternary system of electron donor-mediator (CMK-3)-acceptor was formed. With the help of CMK-3, the activated PS could directly oxidize 2,4-DCP via two-electron conduction (Eq. (6)) without generating free radicals. In this system, radical and non-radical oxidation processes are both involved in the reaction and work together for complete 2,4-DCP decomposition. CMK-3 played crucial roles as the electron transfer mediator to facilitate the transfer of electrons from

pollutants or H$_2$O to PS.

$$S_2O_8^{2-} + 2H_2O \rightarrow HO_2^- + 2SO_4^{2-} + 3H^+ \tag{3}$$

$$S_2O_8^{2-} + HO_2^- \rightarrow SO_4^{2-} + SO_4^{•-} + O_2^{•-} + H^+ \tag{4}$$

$$SO_4^{•-} + OH^- \rightarrow SO_4^{2-} + •OH \tag{5}$$

$$S_2O_8^{2-} + 2e^- \rightarrow 2SO_4^{2-} \tag{6}$$

To further verify the proposed pathway, linear sweep voltammetry (LSV) was used to investigate the electron transfer process. When bar GCE acted as the working electrode, there was no apparent current response in the electrolyte containing both PS and 2,4-DCP (Fig. 6a), which suggested that electron transfer at the electrode interface was very slow. Bar GCE owned very large semicircle diameter in the EIS plot (Fig. 6b), showing the high resistance, which was why the weak oxidation peak of 2,4-DCP could not be found. Owning to the superior electrical conductivity of CMK-3, the resistance of CMK-GCE decreased significantly as the ESI plot was almost a straight line. It could be

Scheme 1. Proposed mechanism of persulfate activation on ordered mesoporous carbon.
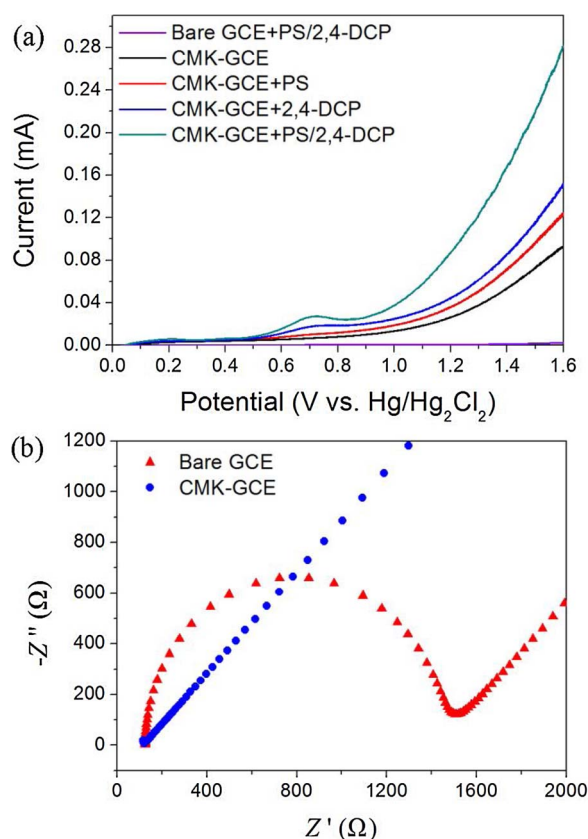
Fig. 6. (a) Linear sweep voltammograms obtained by the bare electrode (bare GCE) and CMK-3 electrode (CMK-GCE) in the presence of PS or 2,4-DCP, [2,4-DCP] = 200 mg/L, [PS] = 2 g/L, 20 mM phosphate buffer at pH = 7; (b) EIS Nyquist plots of bare GCE and CMK-GCE with frequency range from 0.01 Hz to 10^5 Hz.

Fig. 7. The effects of (a) pH and (b) chloride ions on 2,4-DCP degradation and insets are the corresponding changes of pseudo-first-order rate constant. Experimental conditions: [2,4-DCP] = 200 mg/L, [PS] = 2 g/L, [CMK-3] = 0.2 g/L, [Temp] = 298 K.

confirmed by the increased current in LSV plot. When working electrode was CMK-GCE, compared with that in original electrolyte, a minor current increase could be observed with the addition of PS or 2,4-DCP alone, which may be attributed to the electron transfer between PS (or 2,4-DCP) and the surface of CMK-3. However, only when PS and 2,4-DCP were both added, an obvious oxidation peak along with a significant current increase could be observed, indicating the accelerated oxidation reaction and fast electron transfer on CMK-3 surface resulting from the establishment of ternary system. This suggested the importance of all parts (CMK-3, PS and 2,4-DCP) in the reaction, and gave a good support to the proposed ternary system.

The degradation products of 2,4-DCP by the CMK-3/PS system have also been identified, and the results are presented in Fig. S7. The peaks at retention time of 11.10 min and 13.65 min corresponded to 2-chloro-1,4-benzoquinone (2-CBQ) and 2,4-DCP, respectively. It was obvious that 2,4-DCP was gradually oxidized and the main product was 2-CBQ, which could be realized in a non-radical oxidation processes as has been proved by Zhang et al. [6] in a PS/CuO system. The convent from 2,4-DCP to 2-CBQ needs two electrons abstraction by oxidant, corresponding to the electrons that PS obtained (Eq. (6)). In addition, it has also been proved in many studies that the attack of radicals on 2,4-DCP could result in the generation of 2-CBQ [55,56]. Thus, the proposed two-pathway mechanism was reasonable. Moreover, no highly chlorinated products were found, suggesting that the generation of radicals was minor and non-radical pathway may be more predominant.

Generally, chemical parameters of solution would greatly affect the reaction by affecting the adsorption or radical generation process. The influences of initial pH were presented in Fig. 7a. The pH of 2,4-DCP solution without any adjustment was 6.37. Interestingly, reaction rates increased when reaction solutions were adjusted to be more acidic or alkaline (Fig. S8a). It could be clearly seen that the adsorption process
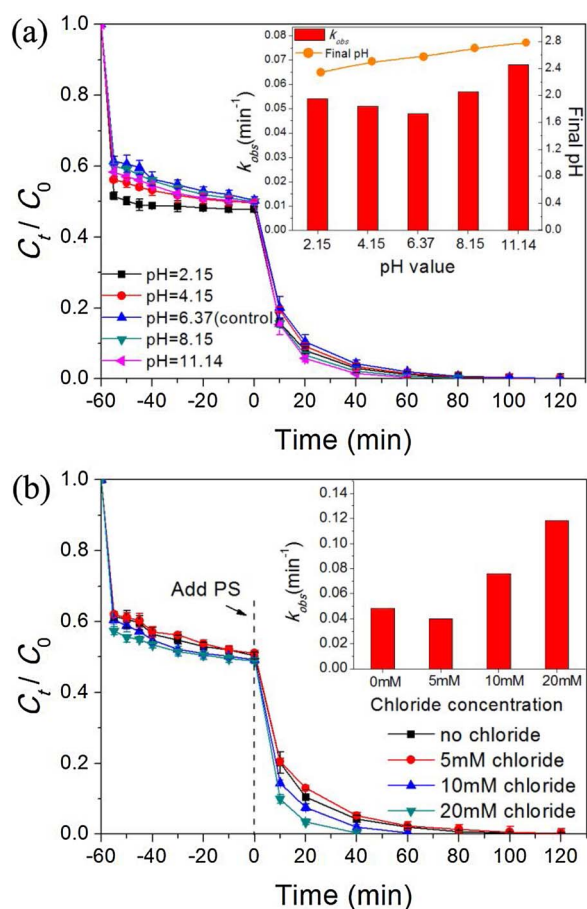
was enhanced with the decrease of pH in acidic condition, which was favorable for the electron transfer as proposed in the mechanism, and thus resulted in an increase in reaction rates. When it comes to alkaline condition, although the adsorption process was not enhanced obviously, the increase of k_{obs} was quite apparent. It is because that the activation of PS can be facilitated in alkaline conditions, where OH^- with negative charge was more easily to donate an electron when compared with H_2O molecules [42]. These results confirmed the roles of radicals in reaction acceleration. The solution pH after reaction was also detected and decreased obviously, owing to the formation of acid intermediates and H^+ (Eqs. (3) and (4)). As a whole, compared with traditional Fenton reaction, CMK-3/PS system remained high activity in a wider pH range, which was favorable for actual water treatment.

Since there are chlorine elements in 2,4-DCP, and chloride ions existing in real wastewater could also act as radical scavengers, the influences of Cl^- on 2,4-DCP degradation by CMK-3/PS was investigated and shown in Figs. 7b and S8b. The presence of 5 mM chloride slightly reduced the degradation rate, because Cl- acted as radical scavengers and combined with $SO_4\cdot^-$ and $\cdot OH$ to form $Cl\cdot$ and $Cl_2\cdot^-$ (Eqs. (7)–(10) [57,58]), which possess lower redox potential than $SO_4\cdot^-$ and $\cdot OH$. However, when the concentration of chloride continued to increase to 10 mM and 20 mM, a distinct increase of k_{obs} could be observed rather than a decrease. According to the proposed mechanism, electron donor was crucial. Here, besides scavenging $SO_4\cdot^-$ and $\cdot OH$, superabundant Cl^- with negative charge could also serve as electron donor to donate electrons to PS, resulting in the generation of active chlorine species and sulfate radicals under the catalysis of CMK-3, which replaced the roles of H_2O in the proposed mechanism. The excess active chlorine species could also take part in the oxidation of
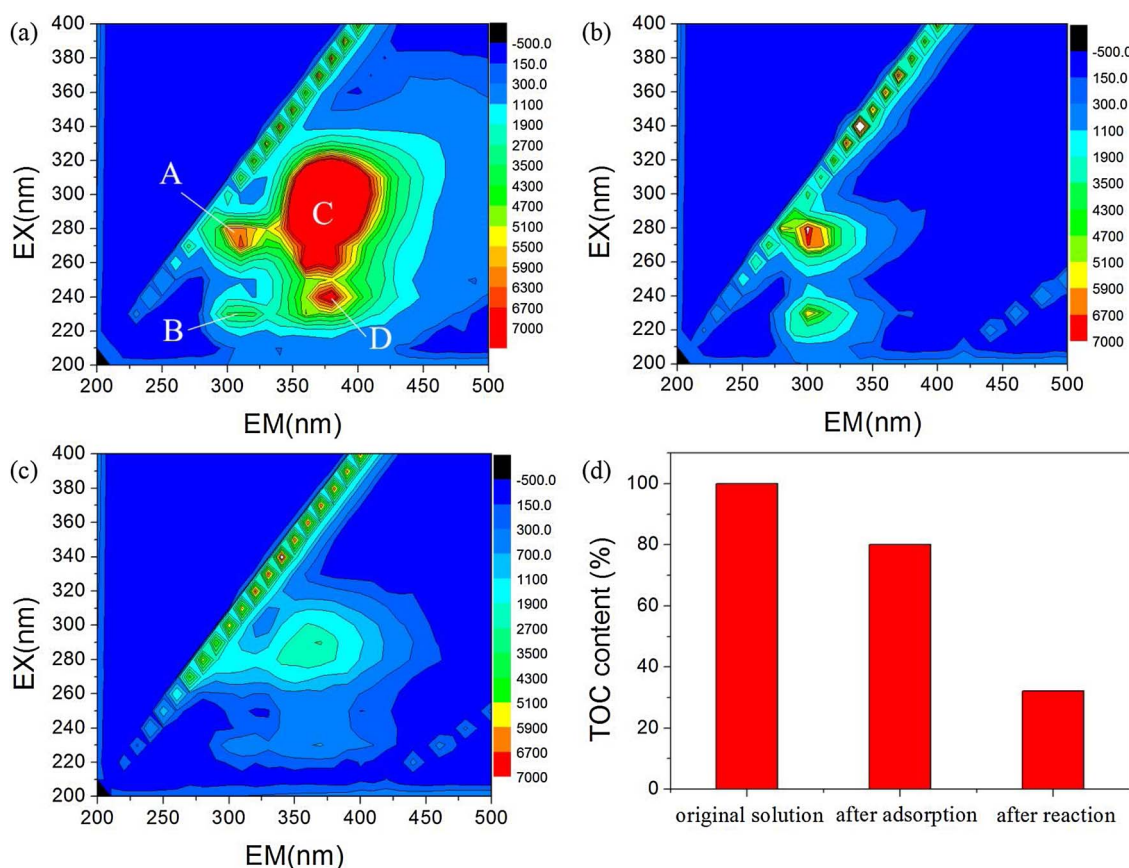
Fig. 8. Three-dimensional excitation and emission matrix (3D-EEM) fluorescence spectroscopy of (a) the original water sample, (b) the sample after adsorption by CMK-3 for 1 h and (c) the sample after reaction with CMK-3/PS for 2 h; (d) the total organic carbon (TOC) changes of the real water sample. Reaction condition: [PS] = 2 g/L, [CMK-3] = 0.2 g/L, [Temp] = 298 K.

2,4-DCP. By promoting radical process, the reaction was accelerated. Based on aforementioned results and discussion, providing an appropriate electron donor should be a feasible approach to improve reaction efficiency in a carbon/PS system. Other methods to promote radical process should also be investigated in future studies.

$$SO_4^{\circ-} + Cl^- \rightarrow Cl^\circ + SO_4^{2-} \tag{7}$$

$$^\circ OH + Cl^- \rightarrow ClOH^{\circ-} \tag{8}$$

$$ClOH^{\circ-} + H^+ \rightarrow Cl^\circ + H_2O \tag{9}$$

$$Cl^\circ + Cl^- \rightarrow Cl_2^{\circ-} \tag{10}$$

3.6. Real wastewater application

Realistic pharmaceutical wastewater was preliminarily used as a target to test whether the system could exhibit high degradation activity in a complex environment containing various organic compounds, and results are presented in Fig. 8. 3D EEM fluorescence spectra is a sensitive technique to determine dissolved organic matter in water and the degree of organic pollution. Four main peaks could be identified from spectra of original sample (Fig. 8a), which were located at Ex/Em of 267–281/297–320 nm (peak A), 225–232/297–320 nm (peak B), 257–318/350–400 nm (peak C) and 235–247/250–400 nm (peak D), respectively. The multiple peaks showed complex components of the water with high concentrations. Peak C and D with high fluorescence intensities were associated with fulvic-like compounds, which indicated the poor biodegradability and serious pollution of the sample, while peak A and B were labeled as protein-like substances [59,60]. After adsorption process, peak C and D disappeared (Fig. 8b).

It was revealed that fulvic-like compounds were adsorbed by CMK-3 while protein-like substances were not. After 2 h reaction with CMK-3/PS (Fig. 8c), peak A and B almost disappeared indicating the oxidation of protein-like substances. Meanwhile, peak C and D reappeared with a low intensity owing to desorption of fulvic-like compounds. On the whole, dissolved organic matters were nearly removed after treatment, resulting in significant improvement in biodegradability of the water. To further confirm the degree of mineralization, TOC measurement was conducted. The results showed that only 20% of pollutants were adsorbed, and about 67.8% of organic pollutants (including the contribution of adsorption) were removed after only 2 h reaction (Fig. 8d), suggesting the high removal efficiency of organics, although part of the TOC reduce may result from the adsorption of reaction intermediates on CMK-3. These results indicated that using CMK-3 to activate persulfate could be an alternative method to deal with practical pharmaceutical wastewater.

The degradation of 2,4-DCP in this real pharmaceutical water sample was also carried out and shown in Fig. S9. Under the disturbance of various compounds, effective decomposition of 2,4-DCP could still achieve with a removal rate of 97% after 2 h reaction. However, compared with that in ultrapure water, k_{obs} decreased from 0.048 min^{-1} to 0.0234 min^{-1}. According to the proposed mechanism, methanol and ethanol existing in wastewater could quench $SO_4 \cdot^-$ and $\cdot OH$, and thus block the radical pathway, resulting in a lower reaction rate. Moreover, other organic components could compete with 2,4-DCP for active sites and radicals, making the degradation of 2,4-DCP slower.

4. Conclusions

In summary, CMK-3/PS system have great application potential in

organic wastewater treatment owing to the high efficiency and stability, providing a novel and effective strategy to develop metal-free catalysts for green remediation. The results indicate that large adsorption capacity of CMK-3 would accelerate the electron transfer, which is favorable for PS activation, and thus result in high catalytic efficiency. Defective sites and functional groups (especially C–OH) on CMK-3 were proposed to play important roles in the catalytic reaction and may act as active sites. Different from conventional activated-persulfate systems, radical and non-radical oxidation processes were found to be both involved in the CMK-3/PS system and worked together for complete 2,4-DCP decomposition. The detailed electron transfer pathways were also proposed. This research gives an in-depth insight to the CMK-3/PS system and provides a novel viewpoint for further PS activation mechanism studies.

Acknowledgments

Appendix A. Supplementary data

Supplementary material related to this article can be found, in the online version, at doi:https://doi.org/10.1016/j.apcatb.2018.02.059.

References

[1] E. Neyens, J. Baeyens, J. Hazard. Mater. 98 (2003) 33–50.
[2] J. Tang, L. Tang, H. Feng, G. Zeng, H. Dong, C. Zhang, B. Huang, Y. Deng, J. Wang, Y. Zhou, J. Hazard. Mater. 320 (2016) 581–590.
[3] G.P. Anipsitakis, D.D. Dionysiou, Environ. Sci. Technol. 37 (2003) 4790–4797.
[4] L. Tang, H. Feng, J. Tang, G. Zeng, Y. Deng, J. Wang, Y. Liu, Y. Zhou, Water. Res. 117 (2017) 175–186.
[5] W.D. Oh, Z. Dong, T.T. Lim, Appl. Catal. B: Environ. 194 (2016) 169–201.
[6] T. Zhang, Y. Chen, Y. Wang, R.J. Le, Y. Yang, J.P. Croué, Environ. Sci. Technol. 48 (2014) 5868–5875.
[7] P. Avetta, A. Pensato, M. Minella, M. Malandrino, V. Maurino, C. Minero, K. Hanna, D. Vione, Environ. Sci. Technol. 49 (2014) 1043–1050.
[8] T.T. Lim, P.S. Yap, M. Srinivasan, A.G. Fane, Crit. Rev. Environ. Sci. Technol. 41 (2010) 1173–1230.
[9] R. Matta, S. Tlili, S. Chiron, S. Barbati, Environ. Chem. Lett. 9 (2011) 347–353.
[10] S. Wacławek, H.V. Lutze, K. Grübel, V.V.T. Padil, M. Černík, D.D. Dionysiou, Chem. Eng. J. 330 (2017) 44–62.
[11] C. Luo, J. Jiang, J. Ma, S. Pang, Y. Liu, Y. Song, C. Guan, J. Li, Y. Jin, D. Wu, Water. Res. 96 (2016) 12–21.
[12] Y.H. Guan, J. Ma, X.C. Li, J.Y. Fang, L.W. Chen, Environ. Sci. Technol. 45 (2011) 9308–9314.
[13] J.M. Monteagudo, A. Durán, R. González, A.J. Expósito, Appl. Catal. B: Environ. 176–177 (2015) 120–129.
[14] Y. Ji, C. Dong, D. Kong, J. Lu, Q. Zhou, Chem. Eng. J. 263 (2015) 45–54.
[15] C. Cai, H. Zhang, X. Zhong, L. Hou, J. Hazard. Mater. 283 (2015) 70–79.
[16] O.S. Furman, A.L. Teel, R.J. Watts, Environ. Sci. Technol. 44 (2010) 6423–6428.
[17] M. Ahmad, A.L. Teel, R.J. Watts, Environ. Sci. Technol. 47 (2013) 5864–5871.
[18] G. Fang, J. Gao, C. Liu, D.D. Dionysiou, Y. Wang, D. Zhou, Environ. Sci. Technol. 48 (2016) 1902–1910.
[19] G.P. Anipsitakis, D.D. Dionysiou, Appl. Catal. B: Environ. 54 (2004) 155–163.
[20] M. Nie, C. Yan, M. Li, X. Wang, W. Bi, W. Dong, Chem. Eng. J. 279 (2015) 507–515.
[21] X. Chen, J. Chen, X. Qiao, D. Wang, X. Cai, Appl. Catal. B: Environ. 80 (2008) 116–121.
[22] E. Saputra, S. Muhammad, H. Sun, A. Patel, P. Shukla, Z.H. Zhu, S. Wang, Catal. Commun. 26 (2012) 144–148.
[23] Y. Feng, J. Liu, D. Wu, Z. Zhou, Y. Deng, T. Zhang, K. Shih, Chem. Eng. J. 280 (2015) 514–524.
[24] P.R. Shukla, S. Wang, H. Sun, H.M. Ang, M. Tadé, Appl. Catal. B: Environ. 100 (2010) 529–534.
[25] H. Sun, S. Liu, G. Zhou, H.M. Ang, M.O. Tadé, S. Wang, ACS Appl. Mater. Interfaces 4 (2014) 5466–5471.
[26] X. Duan, H. Sun, J. Kang, Y. Wang, S. Indrawirawan, S. Wang, Acs. Catal. 5 (2015) 4629–4636.
[27] H. Sun, C.K. Kwan, A. Suvorova, H.M. Ang, M.O. Tadé, S. Wang, Appl. Catal. B: Environ. 154–155 (2014) 134–141.
[28] X. Duan, H. Sun, Y. Wang, J. Kang, S. Wang, Acs. Catal. 5 (2015) 553–559.
[29] S. Indrawirawan, H. Sun, X. Duan, S. Wang, Appl. Catal. B: Environ. 179 (2015) 352–362.
[30] X. Duan, Z. Ao, D. Li, H. Sun, L. Zhou, A. Suvorova, M. Saunders, G. Wang, S. Wang, Carbon 103 (2016) 404–411.
[31] X. Duan, Z. Ao, L. Zhou, H. Sun, G. Wang, S. Wang, Appl. Catal. B: Environ. 188 (2016) 98–105.
[32] Y. Zhou, J. Jiang, Y. Gao, J. Ma, S.Y. Pang, J. Li, X.T. Lu, L.P. Yuan, Environ. Sci. Technol. 49 (2015) 12941–12950.
[33] H. Cheng, H. Guo, Y. Zhang, W. Xiao, L. Yang, Water. Res. 113 (2017) 80–88.
[34] H. Lee, H.J. Lee, J. Jeong, J. Lee, N.B. Park, C. Lee, Chem. Eng. J. 266 (2015) 28–33.
[35] D. Zhao, Q. Huo, J. Feng, B.F. Chmelka, G.D. Stucky, J. Am. Chem. Soc. 120 (1998) 6024–6036.
[36] S. Jun, S. Hoon Joo, R. Ryoo, M. Kruk, M. Jaroniec, Z. Liu, T. Ohsuna, O. Terasaki, J. Am. Chem. Soc. 122 (2000) 10712–10713.
[37] C. Liang, C.F. Huang, N. Mohanty, R.M. Kurakalva, Chemosphere 73 (2008) 1540–1543.
[38] L. Tang, G. Yang, G. Zeng, Y. Cai, S. Li, Y. Zhou, Y. Pang, Y. Liu, Y. Zhang, B. Luna, Chem. Eng. J. 239 (2014) 114–122.
[39] L. Tang, Y. Cai, G. Yang, Y. Liu, G. Zeng, Y. Zhou, S. Li, J. Wang, S. Zhang, Y. Fang, Appl. Surf. Sci. 314 (2014) 746–753.
[40] Y. Zhou, L. Tang, G. Yang, G. Zeng, Y. Deng, B. Huang, Y. Cai, J. Tang, J. Wang, Y. Wu, Catal. Sci. Technol. 6 (2016) 1930–1939.
[41] A. Dabrowski, P. Podkościelny, Z. Hubicki, M. Barczak, Chemosphere 58 (2005) 1049–1070.
[42] X. Duan, C. Su, L. Zhou, H. Sun, A. Suvorova, T. Odedairo, Z. Zhu, Z. Shao, S. Wang, Appl. Catal. B: Environ. 194 (2016) 7–15.
[43] M.A. Alshamsi, N.R. Thomson, Ind. Eng. Chem. Res. 52 (2016) 13564–13571.
[44] L. Tang, G.D. Yang, G.M. Zeng, Y. Cai, S.S. Li, Y.Y. Zhou, Y. Pang, Y.Y. Liu, Y. Zhang, B. Luna, Chem. Eng. J. 239 (2014) 114–122.
[45] P. Neta, R.E. Huie, A.B. Ross, J. Phys. Chem. Ref. Data 17 (1979) 1027–1284.
[46] J.H. Almeida, D.A. Bertuol, A. Meneguzzi, C.A. Ferreira, F.D.R. Amado, Mater. Res. 16 (2013) 860–866.
[47] G.V. Buxton, J. Phys. Chem. Ref. Data. 17 (1988) 513–886.
[48] P.S. Rao, E. Hayon, J. Phys. Chem. 79 (1975) 397–402.
[49] Y. Wang, H. Sun, H.M. Ang, M.O. Tadé, S. Wang, Appl. Catal. B: Environ. 164 (2015) 159–167.
[50] J. Wang, L. Tang, G. Zeng, Y. Deng, H. Dong, Y. Liu, L. Wang, B. Peng, C. Zhang, F. Chen, Appl. Catal. B: Environ. 222 (2018) 115–123.
[51] C. Qi, X. Liu, J. Ma, C. Lin, X. Li, H. Zhang, Chemosphere 151 (2016) 280–288.
[52] E.T. Yun, H.Y. Yoo, H. Bae, H.I. Kim, J. Lee, Environ. Sci. Technol. 51 (2017) 10090–10099.
[53] E. Howard Jr., L.S. Levitt, J. Am. Chem. Soc. 75 (1953) 6170–6173.
[54] H. Liu, T.A. Bruton, W. Li, J.V. Buren, C. Prasse, F.M. Doyle, D.L. Sedlak, Environ. Sci. Technol. 50 (2016) 890–898.
[55] L. Xu, J. Wang, Appl. Catal. B: Environ. 123–124 (2012) 117–126.
[56] W. Chu, C.Y. Kwan, K.H. Chan, S.K. Kam, J. Hazard. Mater. 121 (2005) 119–126.
[57] Y. Yang, J. Jiang, X. Lu, J. Ma, Y. Liu, Environ. Sci. Technol. 49 (2015) 7330–7339.
[58] G.P. Anipsitakis, D.D. Dionysiou, M.A. Gonzalez, Environ. Sci. Technol. 40 (2006) 1000–1007.
[59] L. Wang, Y. Qi, D. Wang, X. Li, G. Zeng, Z. Li, Y. Deng, J. Liu, K. Yi, J. Hazard. Mater. 318 (2016) 460–467.
[60] J. Liu, Q. Yang, D. Wang, X. Li, Y. Zhong, X. Li, Y. Deng, L. Wang, K. Yi, G. Zeng, Bioresource. Technol. 206 (2016) 134–140.